Dual-Polarization Radar Observations of Vortices and Cellular Convection within Lake-Effect Snow Bands

Timothy Cermak, Jeffrey Frame, Eric Ahasic
Department of Atmospheric Sciences, University of Illinois at Urbana-Champaign, Urbana, IL

1. Introduction

Lake-effect snow events have long been a focus of atmospheric research, dating back to at least the 1950's (e.g., Petterssen and Calabrese 1959; Peace and Sykes 1966; Holroyd 1971; Jiusto and Kaplan 1972) and continuing through the present day (e.g., Laird and Kristovich 2004; Barthold and Kristovich 2011). These studies have typically focused on either forecasting lake-effect snow events or modeling mesoscale structures of lake-effect snow bands.

Continued research on lake-effect snow is motivated by the significant societal impacts of these events on effected communities, which for this specific study are located just east and southeast of Lake Ontario. This is one of the snowiest regions east of the Rocky Mountains, with some locations, such as the Tug Hill Plateau of New York, typically receiving over 200 inches of snow annually. Syracuse, NY, a city of almost 150,000 residents and located 35 miles southeast of Lake Ontario, boasts an average annual snowfall of 115.6 inches. The annual snowfall average at Syracuse significantly exceeds that of Albany, NY, which is located 140 miles southeast of Lake Ontario and only has an average annual snowfall of 63.9 inches. Communities affected by lake-effect snow are more vulnerable to societal impacts caused by large snowfall amounts, including increased cost of clearing roads, increased number of automobile accidents, and long lasting power outages. One notable lake-effect event occurred between 3-12 February 2007 and produced staggering snowfall totals, including 141 inches of snow in Redfield, NY, over the 10-

day period. It is because of these astounding snowfall rates and totals that lake-effect snow events are becoming increasingly important topics of research.

Lake-effect convective organization is related to wind speed and direction, lake shape, and vertical wind shear (e.g., Niziol et al. 1995; Markowski and Richardson 2010). Variations among these parameters result in different types of snow bands, and can influence the formation of cellular convection near the bands as well. Lake-effect convection typically organizes into banded structures, but environments characterized by weak vertical wind shear could support cellular convection. The angle at which the wind crosses the lake plays a significant role in the organization of banded structures; if the wind is parallel to the major axis, a single heavy band of precipitation is likely to form. These snow bands are classified as Type I bands (Niziol et al. 1995), and typically produce the heaviest snowfall totals, which tend to be concentrated within a local area. Locations perhaps 10-20 km from the center of the band may receive little or no precipitation from this type of snow band. The second common archetype of lake-effect snow bands occurs when wind blows parallel to the minor axis of a lake. These conditions tend to favor several parallel, but less intense, snow bands (Type II; Niziol et al. 1995). The organization of these bands, dominated by boundary layer roll dynamics, is similar to that of horizontal convective rolls (HCRs). Although these bands typically produce smaller snowfall accumulations, they can cover much larger areas than major-axis parallel bands.

In this study, a dual-polarization Doppler on Wheels (DOW) radar (Wurman et al. 1997) collected data on long-lake axis parallel lake-effect snow bands over Lake Ontario during the winter of 2010-2011. The focus of this study is on possible relationships between dual-polarization observations and the presence of vortices, cellular convection, and banded convection within these snow bands. Data and observations presented in this paper were taken from two specific deployments: 4 January 2011 and 9-10 February 2011. The use of mobile dual-polarization radars in lake-effect snow research is relatively new, because previous studies utilizing dual-polarization radars focused primarily on events unrelated to lake-effect snow, such as warm-season convection (e.g., Frame et al 2009). Other previous studies have utilized dual-polarization radar data for bulk hydrometeor classification and quantification (e.g., Liu and Chandrasekar 2000), but these studies also focused on warm-season convective events. A concurrent study relating dual-polarization observations and surface precipitation data collected during these lake-effect snow events (Ahasic et al. 2012) provides insight into possible relationships between dual-polarization parameters and precipitation types and intensities recorded at the surface.

The synoptic weather patterns for each case are discussed in the following section. The methods by which data were collected, analyzed, and edited during this study are discussed in Section 3. Section 4 explains the results found during this study, and whether these were found to be significant. A summary of the study and its findings, as well as additional questions and suggested topics of further research can be found in section 5.

2. Synoptic Overview

In both cases examined herein, the synoptic-scale weather pattern proved favorable for long-lake axis parallel lake-effect snow band formation over Lake Ontario. Temperatures at 850 mb ranged from -10˚C to -18˚C, and the circulation around low pressure systems over eastern Canada provided westerly winds of sufficient strength over the lake (Fig. 1). These winds were parallel to the major axis of Lake Ontario, which is oriented east-west, generating a long-lake axis parallel fetch. As the cold air flowed over the warm lake, heat and moisture were transferred from the lake to the atmospheric boundary layer, destabilizing the lower atmosphere. This instability, along with the long-axis parallel orientation of the fetch, caused primarily Type I snow bands to form (Niziol et al. 1995).

a) b)

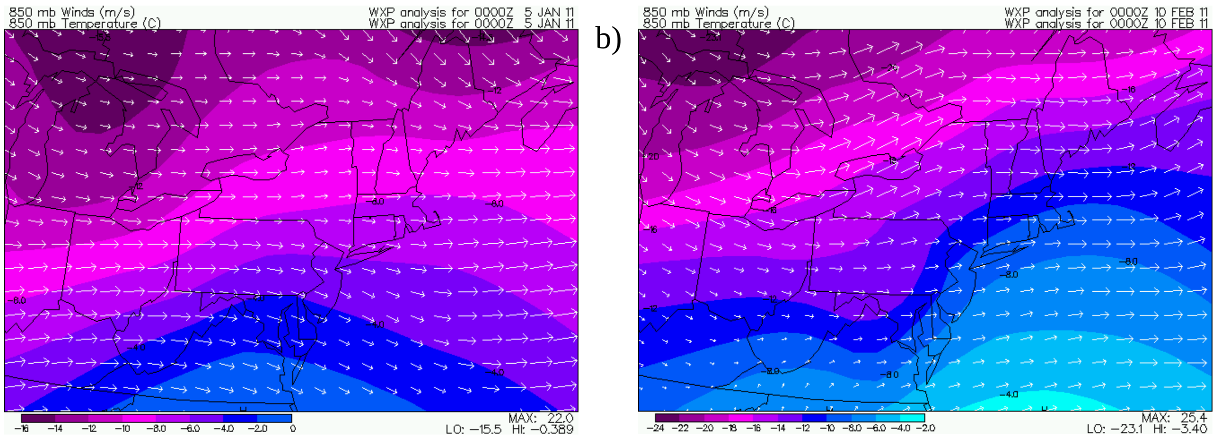

Figure 1: 850 mb analyses for (a) 00 UTC 5 January 2011 and (b) 00 UTC 10 February 2011 temperature (˚C, shaded) and winds (vector). Note that the shading differs between the two panels. Figures courtesy of Plymouth State University

a) b)

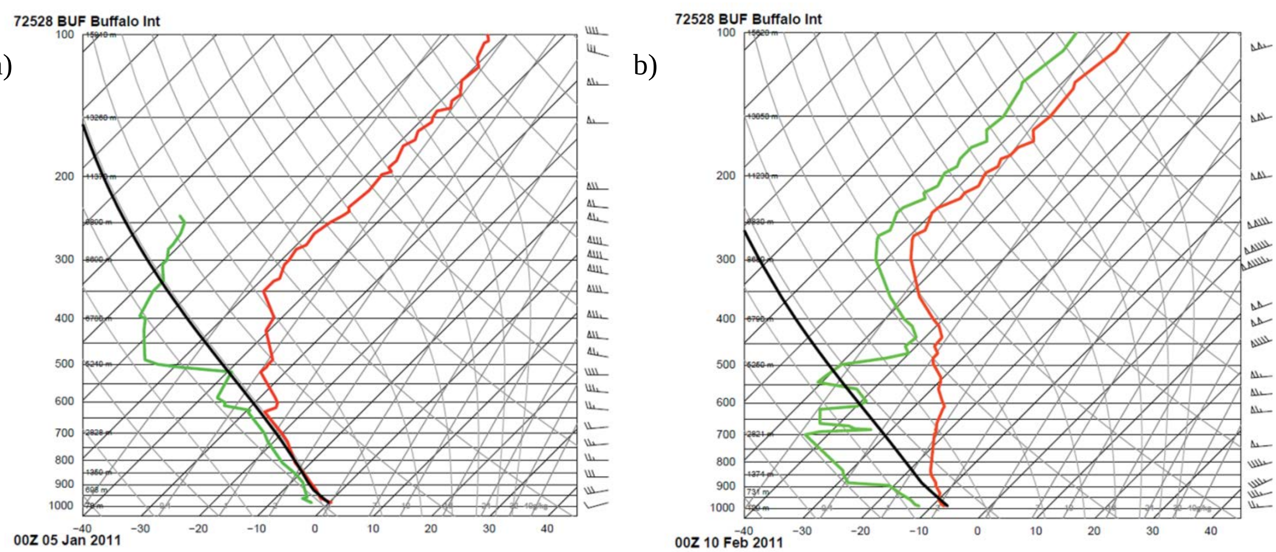

Figure 2: Soundings taken at Buffalo, NY, at (a) 00 UTC 5 January 2011 and (b) 00 UTC 10 February 2011. Plotted are temperature (˚C) in red, dewpoint (˚C) in green, and the temperature (˚C) of an unmodified air parcel lifted from the surface in black. Figures courtesy of the University of Wyoming.

Soundings taken at Buffalo, NY, during these events are provided in Fig. 2. Since Buffalo is upwind of Lake Ontario, these soundings are not necessarily representative of the lakemodified atmosphere downwind of the lake. The inversion at the top of the boundary layer was around 825-850 mb in the 9-10 February 2011 case, but was significantly higher in the 4 January 2011 case, at about 650 mb. Warmer lake temperatures and weaker surface winds during the 4 January 2011 case allowed the lower atmosphere to destabilize more than during the other cases, which, when combined with the higher inversion height, allowed for deeper convection to occur during that case.

3. Data and Analysis

Data from the two cases examined herein were collected using a 3 cm X-band radar (Wurman et al. 1997) with dual-polarization capabilities and a beam width of 0.93˚. During the 4 January 2011 case, the data were collected on the shore of Lake Ontario just west of Fair Haven, NY. On 9-10 February 2011, the data were collected on the shore just southwest of Oswego, NY. Soundings were also launched at various locations and times to obtain more accurate real-time vertical profiles of the atmosphere.

SOLOII (Oye et al. 1995) software was used to view, analyze, and later edit Plan Position Indicator (PPI) and Range Height Indicator (RHI) scans taken during each deployment. PPI volume scans typically consisted of 11 or 12 elevation scans, ranging from 1.0˚ to 11.0˚ for the 4 January 2011 case, and from 0.3˚ to 10.3˚ for the 9-10 February 2011 case. Exceptions were made in specific situations during which certain elevation scans would be repeated to track an interesting feature, such as a vortex, more quickly and accurately. RHI scans varied in size and spacing between individual scan azimuths, depending on the location of the primary snow band and any vortices or cellular convection relative to the location of the radar. For the majority of each deployment, however, scans regularly alternated between PPI and RHI.

As mentioned earlier, the use of dual-polarization radars during lake-effect snow events has been relatively unexplored, so the opportunity presented to analyze dual-polarization data was novel. The conventional variables focused on are horizontal reflectivity (Z_H) and radial velocity (V_R). The dual-polarization variables focused on are differential reflectivity (Z_{DR}), specific differential phase (K_{DP}), and the cross-correlation coefficient between the horizontally and vertically polarized waves (ρ_{hv}). Differential reflectivity is the logarithm of the ratio of power returned from horizontally polarized pulses to that returned from vertically polarized pulses. This means that objects with large aspect ratios will tend to have larger values of Z_{DR}, while more spherical objects will typically exhibit Z_{DR} values closer to zero. Specific differential phase is the range derivative of the differential phase shift between the horizontally and vertically polarized pulses. As a radar pulse travels through hydrometeors, the speed of the pulse is affected by the water content in its path. The phase shift caused by this change in pulse speed is measured, and can then be related to the water content along the path of the radar beam. Typically, large values of K_{DP} indicate the presence of hydrometeors with high liquid water contents, while values close to zero indicate small liquid water contents. The cross-correlation coefficient between the horizontally and vertically polarized waves (ρ_{hv}) can be used to determine hydrometeor type, because values of ρ_{hv} are typically near unity if the radar pulse only encounters hydrometeors of the same type, Lower values of ρ_{hv} are usually related to a mixture of hydrometeors within a pulse volume, because mixed hydrometeor types scatter horizontally and vertically polarized waves differently.

Most dual-polarization fields were difficult to interpret using SOLOII alone. Noise caused by ground clutter, second trip echoes, beam blockage, and areas of poor-quality data were removed using the SOLOII editing widget. Even after editing the data, however, it often proved difficult to interpret many of the dual-polarization fields. To help further analyze these parameters, Barnes (1964) objective analyses of volume scans containing interesting features (e.g., vortices) were performed using REORDER (Oye and Case 1992).

Important objective analysis parameters, such as grid spacing, radius of influence, and the weighting parameter for each objective analysis were calculated following Pauley and Wu (1990) and Marquis et al. (2007). The grid spacings Δx, Δy, and Δz were defined following Δx, Δy, Δz = (5/12)δ and the radii of influence for each data point, r_x, r_y, and r_z, were defined using $r_x, r_y, r_z = 3\delta$, in which δ is the maximum observed data spacing in the analysis domain. Finally, the weighting function at each grid point was determined by $\kappa = (1.33\delta)^2$.

Of the objective analyses performed, four are discussed in detail. The first analysis was performed on an area of cellular convection during the 4 January 2011 deployment. Another is of a large vortex during the 4 January 2011 case. The third analysis is for an area where a vortex is present within cellular convection during the 4 January 2011 case, and the final analysis is of cellular convection during the 10 February 2011 case. The objective analysis parameters for each case are provided in Table 1, and the details of these analyses are discussed in the next section.

Constant	
Beam Width, θ	0.93°
4 January 2011 (Figures 3b-d)	
R	43 km
δ	0.688 km
Δx, Δy, Δz	0.287 km
r_x, r_y, r_z	2.065 km
K	0.8378
4 January 2011 (Figure 6)	
R	13 km
δ	0.208 km
Δx, Δy, Δz	0.085 km
r_x, r_y, r_z	0.624 km
K	0.0765
4 January 2011 (Figure 7)	
R	43 km
δ	0.688 km
Δx, Δy, Δz	0.280 km
r_x, r_y, r_z	2.064 km
K	0.837
10 February 2011 (Figures 4b-e)	
R	47 km
δ	0.755 km
Δx, Δy, Δz	0.314 km
r_x, r_y, r_z	2.26 km
K	1.008

Table 1: Objective analysis parameters for each case. See text for description of the variables

4. Results

a) Cellular vs. Banded Convection

A prominent feature in both the 4 January 2011 and 9-10 February 2011 cases is the simultaneous presence of cellular and banded convection. Figure 3 provides an example of cellular convection observed at 01:35:45 UTC 5 January 2011. The cellular convection can be seen organized roughly along the 300° azimuth, just south of the primary snow band (Fig. 3a).

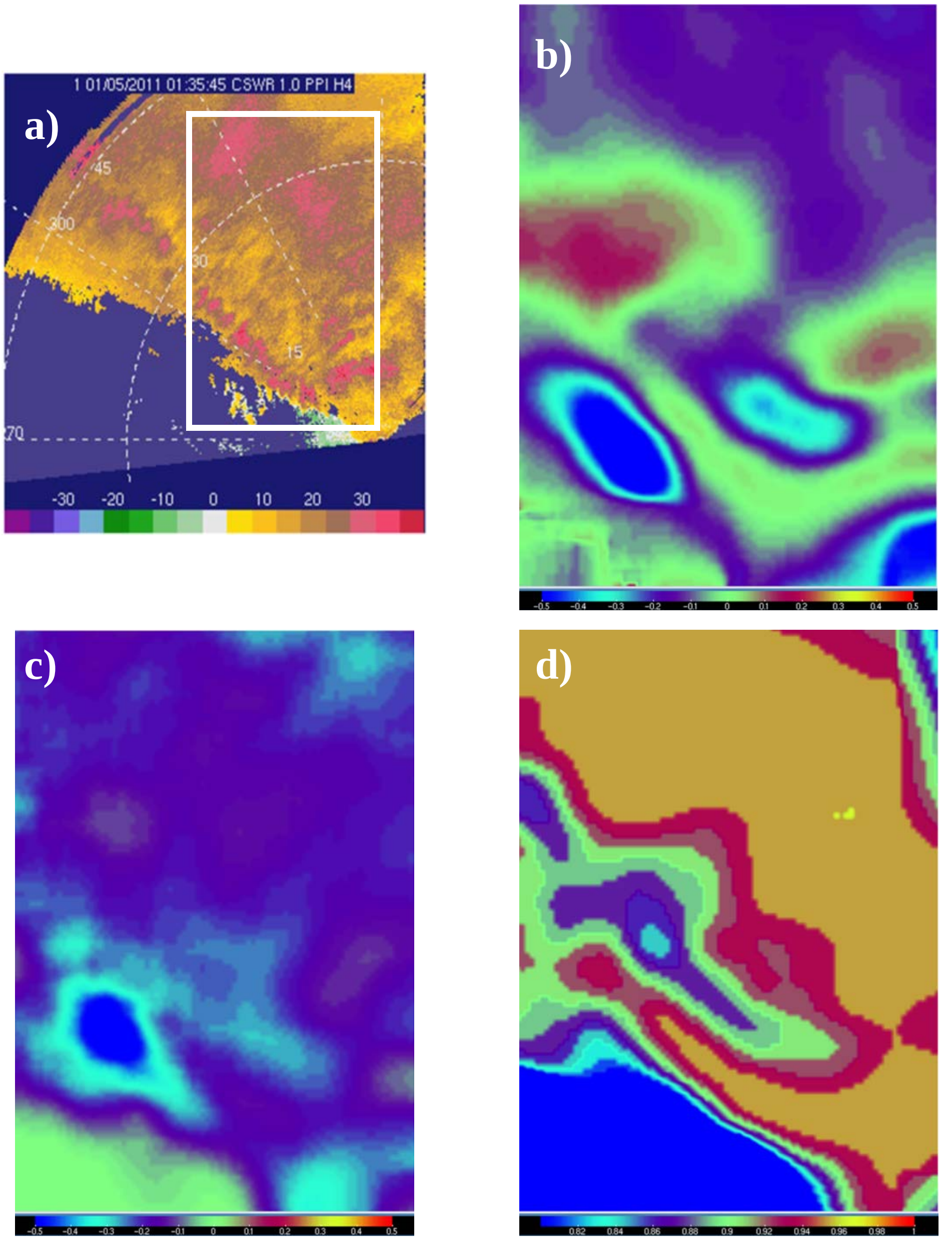

Figure 3: (a) 1.0° elevation Z_H (dBZ) scan from 01:35:45 UTC 5 January 2011 and objective analyses at 287 m above ground level of (b) Z_{DR} (dB), (c) K_{DP} (deg/km), and (d) ρ_{hv} for the white box in (a) between 01:35:30 UTC and 01:37:26 UTC.

It is possible that the surface wind direction relative to the orientation of the primary snow band influences the strength and organization of the convection. During the 4 January 2011 case, convective cells occurred south of the primary band and persisted throughout most of the deployment (Fig. 3a), likely because west-southwesterly near-surface winds enhanced convergence along the southern edge of the primary band. During the 9-10 February 2011 case, the surface winds were more westerly, which could explain the formation of cellular convection on the northwest side of the primary snow band (Fig. 4). Cellular convection was observed in other cases as well, varying in strength and location relative to the primary snow bands. The strongest and most prominent cellular convection occurred during the 4 January 2011 case, however.

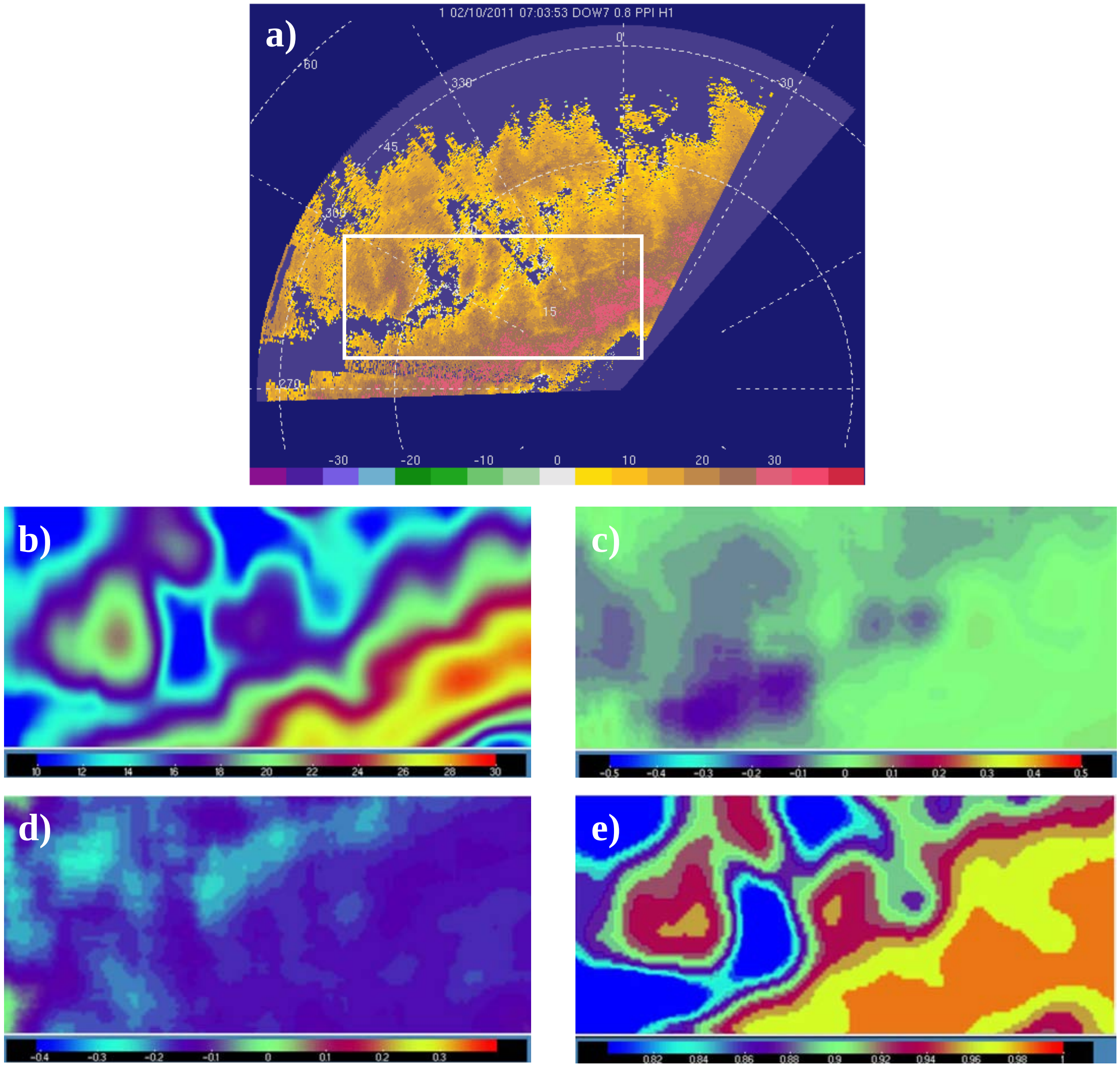

Figure 4: (a) 0.8° elevation Z_H (dBZ) scan from 07:03:53 UTC 10 February 2011 with a white box representing the area in which objective analyses were performed at 314 m above ground level for (b) Z_H (dBZ), (c) Z_{DR} (dB), (d) K_{DP} (deg/km), and (e) ρ_{hv}.

During the 4 January 2011 case, Z_{DR} consistently achieved values between 0.0 and 0.2 dB within the convective cells. The locations of these maxima are significant because there are regions of the primary snow band north of the cellular convection that are not collocated with positive Z_{DR} values (Fig. 3b), but instead with Z_{DR} values roughly between -0.2 and -0.1 dB. It is important to note that reflectivity values in both the convective cells and primary snow band are similar, with values around 30 dBZ at each location (Fig. 3a). Also, this difference in Z_{DR} values was not observed during the 9-10 February 2011 case, during which Z_{DR} values in both the convective cells and primary snow band remained close to zero (Fig. 4c). This difference in Z_{DR} values is likely related to the properties of ice crystals at each location, as discussed below.

Previous studies that focused on the classification of hydrometeor types from dual-polarization observations (e.g., Straka et al. 2000) indicate that a relationship likely exists between Z_{DR} and hydrometeor type and distribution. The Z_{DR} range suggested by Straka et al. for vertically oriented ice crystals was between -0.5 and 0 dB, between 0 and 6 dB for horizontally-oriented ice crystals, and between 0.0 and 0.2 dB for dry aggregates. Following these ranges, the slightly negative values of Z_{DR} found in the primary snow band during the 4 January 2011 case are likely associated with vertically oriented ice crystals, as opposed to the dry aggregates associated with the convective cells. It is also interesting to note that values of Z_{DR} became more negative with height in the primary snow band, while values in the convective cells remained roughly the same (Fig. 5).

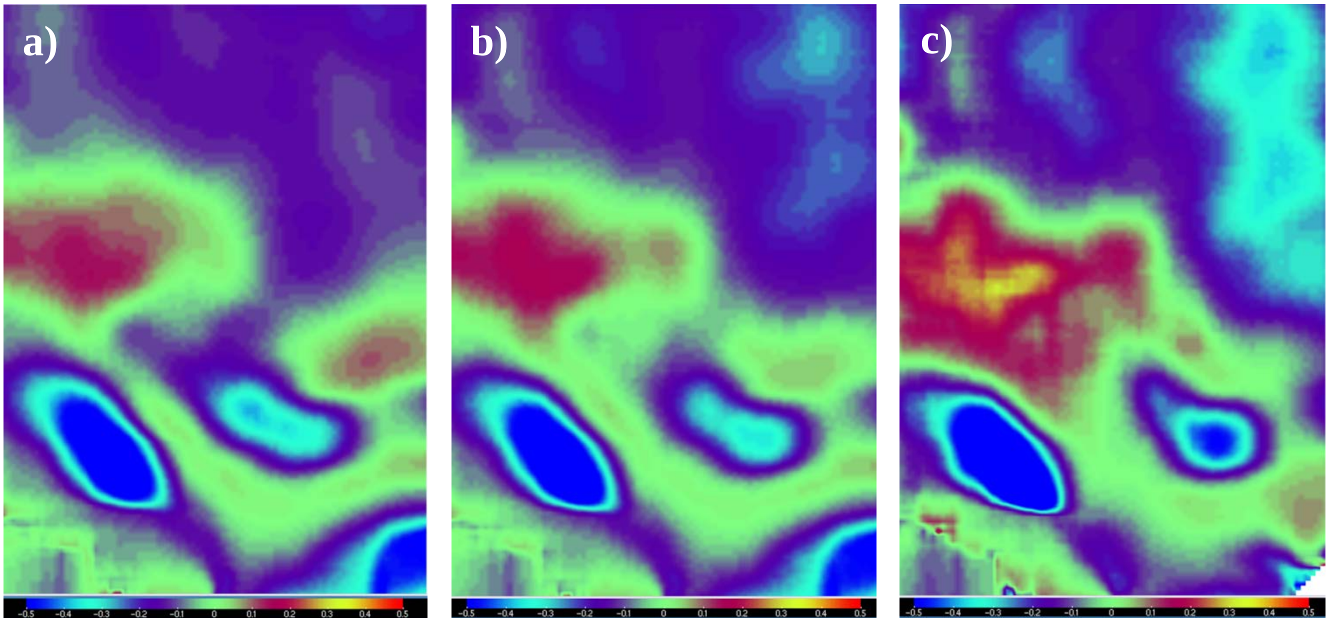

Figure 5: Objective analyses of Z_{DR} (dB) from Fig. 3 at differing vertical levels. Of the 14 vertical levels analyzed, (a) 0.287 km, (b) 1.44 km, and (c) 2.87 km are shown.

Values of K_{DP} typically remained between -0.2 and 0.0 deg/km within both the convective cells and primary bands (e.g., Figs. 3c and 4d). Previous studies (e.g., Ryzhkov and Zrnić 1998; Ryzhkov et al. 1998) utilizing the National Severe Storms Laboratory (NSSL) Cimarron, OK, radar and an instrumented aircraft suggest the presence of horizontally orientated ice crystals if $0.0 < K_{DP} < 0.6$ deg/km and $5 < Z_H < 30$ dBZ, and vertically orientated ice crystals when $0.0 > K_{DP} > -0.6$ deg/km and $5 < Z_H < 30$ dBZ. Therefore, values of K_{DP} between -0.2 and 0.0 deg/km in the convective cells and bands likely indicate ice crystals with a vertical orientation. There were instances, though, during which the convective cells returned K_{DP} values closer to 0.4 deg/km (Fig. 6e). Vivekanandan et al. (1994) observed K_{DP} values in a thunderstorm anvil ranging from 0.25 to 0.5 deg/km, and attributed the values to horizontally aligned crystals mixed with spherical aggregates. This possible hydrometeor type is further supported by Z_{DR} values between 0.0 and 0.2 dB within the convective cells during these times

(Fig. 6d), which, as mentioned earlier, also suggest the presence of dry aggregates and/or horizontally oriented ice crystals.

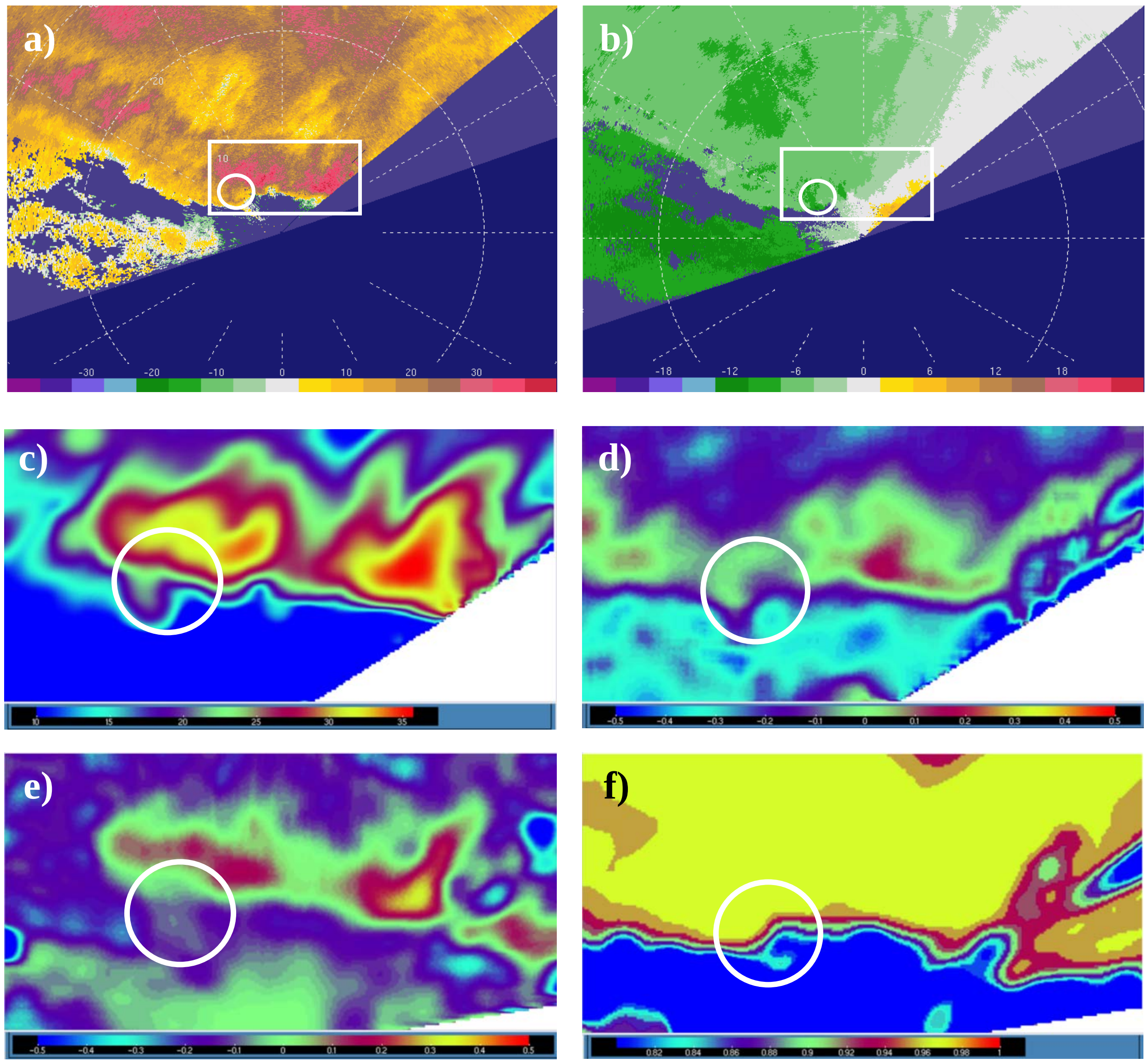

Figure 6: 1.0˚ elevation (a) Z_H (dBZ) and (b) V_R (m/s) scans from 00:03:51 UTC 5 January 2011 and objective analyses of (c) Z_H (dBZ), (d) Z_{DR} (dB), (e) K_{DP} (deg/km), and (f) ρ_{HV} at 85 m above ground level, performed on the area in the white box in (a) and (b). A vortex is circled in (a) through (f).

Values of ρ_{hv} remained between 0.94 and 1.0 in both convective cells and primary snow bands throughout all cases (Figs. 3d, 4e, and 6f). Previous studies (e.g., Balakrishnan and Zrnić 1990) argue that values this close to unity indicate similar hydrometeor orientations and types. A concurrent study (Ahasic et al. 2012) will look deeper into hydrometeor types observed during these deployments, and relate them to the dual-polarization fields.

A deeper, relatively warm and moist layer near the surface during the 4 January 2011 case (Fig. 2a) provided a different environment for ice crystal growth and aggregation processes than that during the 9-10 February 2011 case (Fig. 2b). It is understood that clouds with temperatures between 0˚C and -8˚C contain supercooled water droplets (Wallace and Hobbs 2006, p. 236). During the 4 January 2011 case, lower levels of the clouds fell within this temperature range (Fig. 2a). It is also important to note that temperatures between -10˚C and -18˚C within a cloud favor dendrite formation (Rogers and Yau 1989, p. 162-163), and during the 10 February 2011 case, the clouds contained temperatures below -8˚C at all levels, with a relatively deep layer in the lower levels containing temperatures between -10˚C and -18˚C. Based on these observations, it is expected that the dominant hydrometeor type during the 4 January 2011 case would be pellets, and dendrites would be most common during the 10 February 2011 case. This expectation was confirmed by surface observations taken during these events (Ahasic et al. 2012). Although, given that ice crystals would have been exposed to differing temperatures and supersaturations while falling through the clouds, it is possible crystals with more complex structures existed during both cases as well.

b) Vortices

Vortices were frequently observed in varying locations with respect to the primary snow bands during each deployment. Some formed in the convective cells discussed above, while others were embedded in the snow bands, with a large majority being the latter (Ruth et al. 2012). Although one vortex observed during the 4 January 2011 case had a diameter of about 10 km, most vortices ranged from a few hundred meters to a couple kilometers in diameter. Before considering dual-polarization observations of vortices, the vortices were classified by case, size, and location with respect to the radar. These classifications helped identify possible similarities between dual-polarization signatures of different vortices. Values of the dual-polarization parameters varied between vortices with similar sizes and radar-relative locations. The focus shifted instead toward vortices with similar reflectivity structures, the results of which will be discussed in the following paragraphs.

A common feature associated with the vortices was a hook echo shape in reflectivity, although values of reflectivity in the hook echo often remained below 25 dBZ (e.g., Fig. 4a; Fig. 5; Ruth et al. 2012). There appeared to be a general pattern in the Z_{DR} fields associated with vortices of similar structure in reflectivity. Vortices with a hook reflectivity signature almost always had a Z_{DR} maximum in the hook, although this was likely due to the absence of precipitation near the center of the vortex (Figs. 6a and 6c). Identifying any persistent Z_{DR} signatures for vortices lacking a hook-shaped reflectivity appendage or embedded within a band or cell proved difficult, as dual-polarization observations of these vortices were difficult to distinguish from those of the band or cells in which the vortices were embedded.

Objective analyses significantly improved the K_{DP} fields (e.g., Figs 3c, 4d, and 6f) when compared to the unanalyzed data (e.g., Fig. 6d). Values of K_{DP} in the hook echoes typically followed the patterns those within the convective cells associated with the vortices. For example, in the vortex observed at 00:03:51 5 January 2011, values of K_{DP} are visibly greater, albeit only slightly, than the neighboring areas of no precipitation (Fig. 6e). This difference in values between the hook echo and regions of no precipitation likely only exists because hydrometeors advected into the hook echo by the circulation return values of K_{DP} resembling those nearby in the convective cell, where the hydrometeors likely originated.

In Fig. 7, the 10 km diameter vortex observed at 03:18:13 UTC 5 January 2011 can be seen about 25 km west of the DOW, moving eastward. This vortex is significant not only because of its size and strength, but because of the local Z_{DR} maxima located along its leading edge (Figs. 7b and 7e). Values of Z_{DR} along the leading edge remained between -0.2 and 0.1 dB, as opposed to the Z_{DR} values between -0.5 and -0.3 dB near the center of the vortex. It is possible that locally enhanced near-surface convergence along the leading edge caused stronger updrafts to form. As mentioned above, stronger updrafts support the aggregation and growth of ice crystals into larger, heavier crystals, generally possessing random or nearly spherical orientations. Surface observations recorded regularly at the radar site confirm that hydrometeor type changed from pellets to dendrites immediately after the leading edge of the vortex passed. Snow pellets have been found to return values of Z_{DR} greater than those of dendrites (Ahasic et al. 2012), which further supports the difference between Z_{DR} values at the leading edge and the center of the vortex.

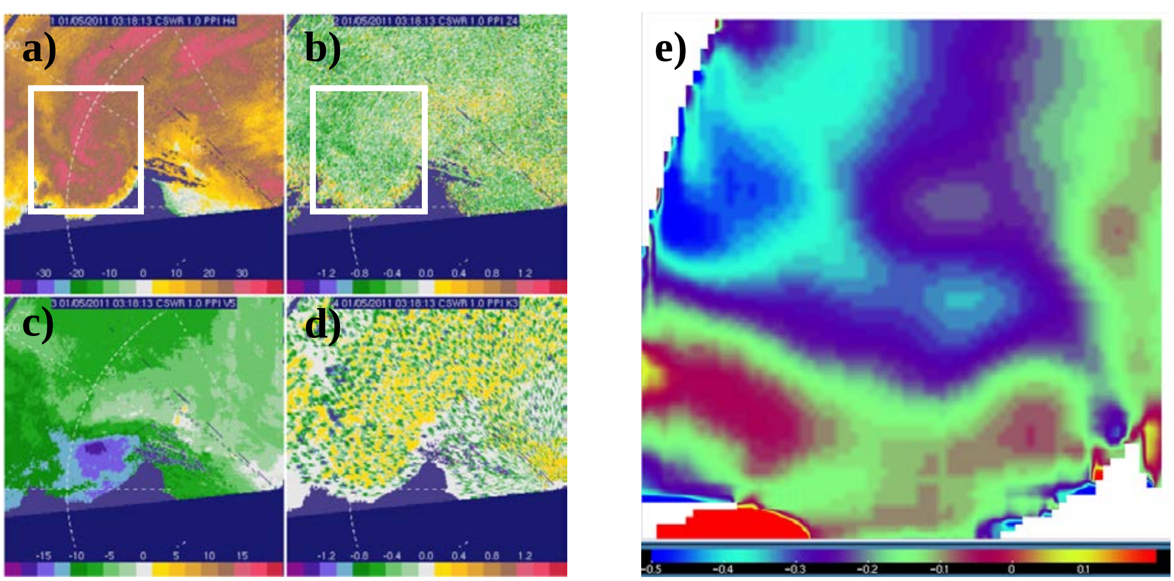

Figure 7: 1.0° elevation scan from 03:18:13 UTC 5 Jan 2011. (a) Z_H (dBZ), (b) Z_{DR} (dB), (c) V_R (m/s), (d) K_{DP} (deg/km), and (e) an objective analysis of Z_{DR} (dB) at 280 m above ground level for the area in the white box.

c) Range Height Indicator Comparisons

Also observed were higher Z_{DR} values located within the upper elevations of the primary band, as opposed to near the surface where the higher reflectivity values tended to be recorded (Fig. 8). Figure 8e shows a 0.3° elevation PPI scan taken at 03:51:37 UTC 10 February 2011, immediately before the RHI scan, with a dashed white line indicating the azimuth along which the RHI was taken. The Z_{DR} maxima in the RHI are located near the top of the clouds (greatest near the suspected updraft). It is well understood that ice crystals with a column-like structure (e.g., needles) have greater terminal velocities than plate-like ice crystals, which are easily carried to high altitudes in updrafts given their flat, horizontal structure (Rogers and Yau 1989, pp. 164-165). Also, hydrometeors with lower aspect ratios will typically return higher values of Z_{DR}. Therefore, the higher Z_{DR} values observed near the top of the clouds likely exist because flat, plate-like ice crystals with small aspect ratios are carried higher into the clouds by the updrafts than the more vertically-oriented columnar ice crystals. Values of ρ_{hv} typically remained between 0.98 and 1.0 throughout the cloud, regardless of elevation (Fig. 8c). It is important to note that because the 4 January 2011 case contained more mixed hydrometeor types, that ρ_{hv} values during that case should be slightly lower than those during the 10 February 2011 case. This is confirmed by an RHI taken through a convective cell from 00:06:27 UTC 5 January 2011 (Figs. 9a-d). Values of ρ_{hv} during this case remain closer to 0.94, instead of the 0.98 – 1.0 seen during the 9-10 February 2011 case. Although slight, the difference is noticeable, and is visible throughout the entire convective cloud.

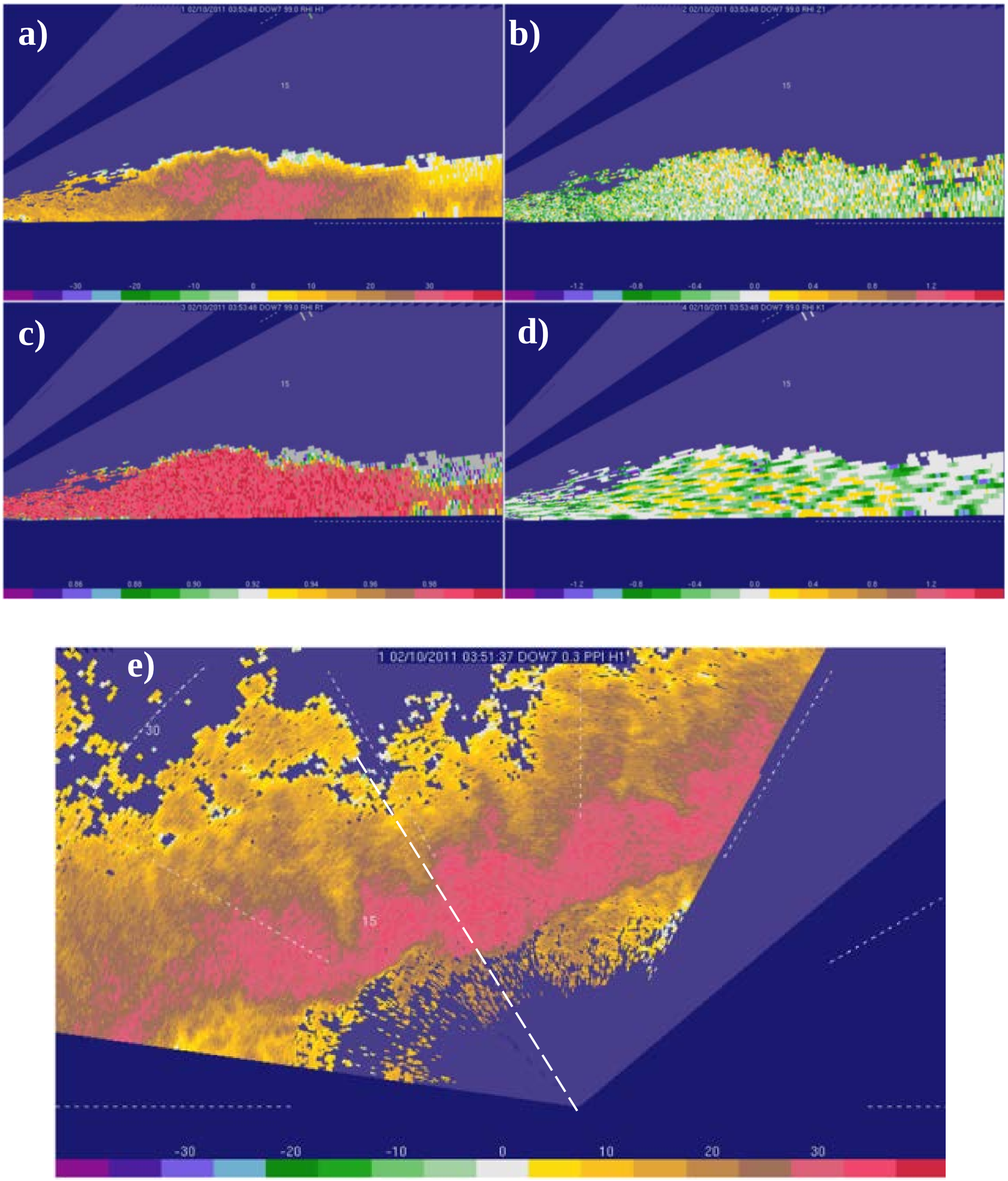

Figure 8: RHI scan from 03:53:48 UTC, 10 February 2011 at a 328° azimuth. Plotted are (a) Z_H (dBZ), (b) Z_{DR} (dB), (c) ρ_{HV}, (d) KDP (deg/km). (e) 0.3° elevation PPI reflectivity scan from 03:51:37 UTC 10 February 2011, immediately before the RHI in (a)-(d) was taken. The dashed line marks the azimuth along which the RHI was taken through the band.

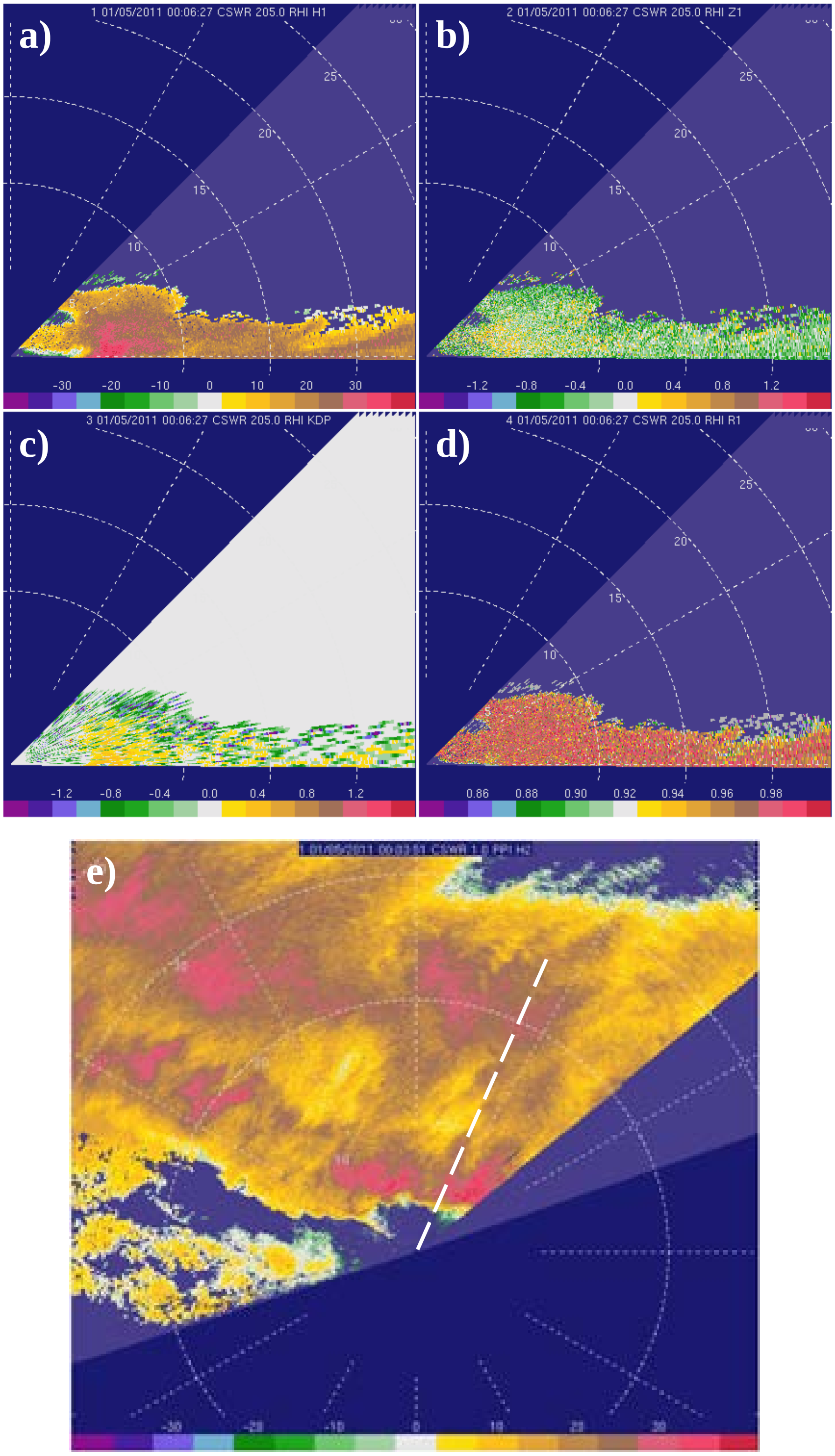

Figure 9: RHI scans from 00:06:27 UTC 5 January 2011, with (a) Z_H (dBZ), (b) Z_{DR} (dB), (c) K_{DP} (deg/km), and (d) ρ_{hv} plotted. (e) 1.0° elevation Z_H (dBZ) PPI scan from 00:03:51 UTC 5 January 2011, with a white dashed line representing the azimuth along which the RHI was taken.

5. Conclusions

Lake-effect snow events have significant impacts have on local communities, including long-lasting power outages, increased risk of automobile accidents, and increased costs of clearing roads and airport runways. This study provides insight as to whether the mesoscale structures of vortices and convection locally affect hydrometeor characteristics and the associated dual-polarization fields. Further research in this topic is important because a more complete understanding of how these mesoscale structures affect hydrometeor characteristics can provide tools for more accurate and detailed short-term lake-effect snow forecasting.

Values of K_{DP} remained similar within convective cells and primary snow bands in most cases, although the occasional stronger convective cell provided slightly higher values of K_{DP} than other, weaker, cells. These stronger cells, however, also typically contained higher values of reflectivity, indicative of more numerous or larger hydrometeors and therefore increased liquid water content. Values of ρ_{hv} near unity were frequently collocated with high reflectivity values within convective cells and bands, although this relationship was found to exist anywhere higher reflectivity values were present, regardless of the location.

During the 4 January 2011 case, values of Z_{DR} were typically higher in convective cells than in the primary snow band, while during the 9-10 February 2011 case, Z_{DR} values remained roughly similar in both the convective cells and primary snow band. Stronger updrafts in convective cells likely supported the formation of hydrometeors oriented differently from those in the primary snow band. Utilizing suggested relationships between ice crystal orientations and Z_{DR} values from previous studies, it was concluded that the convective cells likely contained more horizontally or spherically orientated ice crystals, while the primary band displayed values more representative of vertically orientated ice crystals. Ice crystals with suspected horizontal orientations in the convective cells were also carried aloft more easily in the updrafts of the convective cells than vertically or spherically oriented ice crystals, which explains the observed maxima in Z_{DR} aloft in the cells.

Values of Z_{DR} varied between vortices of different sizes, locations, and deployments. Many vortices possessed a visible hook-like signature in reflectivity, and one frequent observation was heightened values of Z_{DR} in the hook signature of vortices. Vortices embedded within the primary band or convective cells displayed no significant effects on local values of Z_{DR}, likely because any effects would have been difficult to differentiate from the observations of the band or cell itself. High values of K_{DP} and values of ρ_{hv} near unity remained collocated with high values of reflectivity, regardless of whether vortices were present.

Through these analyses of dual-polarization data taken during lake-effect snow events, this study was able to highlight possible effects cellular and banded convection, as well as vortices of varying sizes, have on local dual-polarization and hydrometeor characteristics. It is important to note that this study focused on long lake-axis-parallel lake-effect snow events over Lake Ontario, and that these observations are not necessarily representative of all lake-effect snow events. Further research could focus on different archetypes of lake-effect snow, as well as events over other lakes, within different regions, and occurring in varying meteorological environments. Also, observations utilizing radars of different wavelengths (e.g., K-band) could be of significant use for more detailed dual-polarization and mesoscale structure analyses. Future observations with S-band radars, for example, will become easier to obtain due to the integration of dual-polarization capabilities into the WSR-88D radar network.

Acknowledgements. We are grateful to Dr. Scott Steiger of the State University of New York at Oswego for his assistance with this project and all of the volunteers (too numerous to mention) who helped with the data collection. We also thank Dr. Josh Wurman, Dr. Karen Kosiba, and Justin Walker of the Center for Severe Weather Research for operating the DOW radar and David Wojtowicz of the University of Illinois at Urbana-Champaign for technical assistance. Support from NSF Grant No. AGS10-42854 is also acknowledged.

REFERENCES

Ahasic, E., J. Frame, and T. Cermak, 2012: Classification of precipitation types in lake-effect snow events using dual-polarimetric Doppler radar observations. Preprints, *16th Symposium on Meteorological Observation and Instrumentation*, Amer. Meteor. Soc., New Orleans, LA, paper 6.4.

Balakrishnan, N. and D. S. Zrnic, 1990: Estimation of rain and hail rates in mixed-phase precipitation. *J. Atmos. Sci.*, **47**, 565–583.

Barnes S.L., 1964: A technique for maximizing details in numerical weather map analysis. *J. Appl. Meteor.*, **3**, 396–409.

Barthold, F. E. and D. A. R. Kristovich, 2011: Observations of the cross-lake cloud and snow evolution in a lake-effect snow event. *Mon. Wea. Rev.*, **139**, 2386–2398.

Frame, J., P. Markowski, Y. Richardson, J. Straka, and J. Wurman, 2009: Polarimetric and dual-Doppler radar observations of the Lipscomb County, Texas, supercell thunderstorm on 23 May 2002. *Mon. Wea. Rev.*, **137**, 544–561.

Holroyd, E. W., 1971: Lake-effect cloud bands as seen from weather satellites. *J. Atmos. Sci.*, **28**, 1165–1170.

Jiusto, J. E. and M. L. Kaplan, 1972: Snowfall from lake-effect storms. *Mon. Wea. Rev.*, **100**, 62–66.

Laird, N. F. and D. A. R. Kristovich, 2004: Comparison of observations with idealized model results for a method to resolve winter lake-effect mesoscale morphology. *Mon. Wea. Rev.*, **132**, 1093–1103.

Liu, H. and V. Chandrasekar, 2000: Classification of hydrometeors based on polarimetric radar measurements: Development of fuzzy logic and neuro-fuzzy systems, and in situ verification. *J. Atmos. Oceanic Technol.*, **17**, 140–164.

Markowski, P. M., and Y. P. Richardson, 2010: *Mesoscale Meteorology in Midlatitudes*. Wiley-Blackwell, 407 pp.

Marquis, J., Y. P. Richardson, and J. M. Wurman, 2007: Kinematic observations of misocyclones along boundaries during IHOP. *Mon. Wea. Rev.*, 135, 1749–1768.

Niziol, T. A., W. R. Snyder, and J. S. Waldstreicher, 1995: Winter weather forecasting throughout the Eastern United States. Part IV: Lake effect snow. *Wea. Forecasting*, **10,** 61–77.

Oye, R. and M. Case, 1992: REORDER— A program for gridding radar data: Installation and use manual for the UNIX version. NCAR, 22 pp

Oye, R., C. Mueller, and S. Smith, 1995: Software for radar data translation, visualization, editing, and interpolation. Preprints, *27th Conf. on Radar Meteorology*, Amer. Meteor. Soc., Vail, CO.

Pauley, P. M. and X. Wu, 1990: The theoretical, discrete, and actual response of the Barnes objective analysis scheme for one- and two-dimensional fields. *Mon. Wea. Rev.*, **118,** 1145–1164.

Peace, R. L. and R. B. Sykes, 1966: Mesoscale study of a lake effect snow storm. *Mon. Wea. Rev.*, **94**, 495–507.

Petterssen, S. and P. A. Calabrese, 1959: On some weather influences due to warming of the air by the Great Lakes in winter. *J. Meteor.*, **16**, 646–652.

Rogers, R. R. and M. K. Yau, 1989: *A Short Course in Cloud Physics*, *3rd* ed., Butterworth Heinemann, 290 pp.

Ruth, D. J., K. D. Jaszka, B. W. Rathbun, R. S. Schrom, T. J. Kress, S. Steiger, and A. Stamm, 2012: Investigating the structure of long lake-axis-parallel lake-effect snow bands with a Doppler on Wheels. Preprints, *16th Symposium on Meteorological Observations and Instrumentation*, Amer. Meteor. Soc., New Orleans, LA, paper 6.1.

Ryzhkov, A. and D. S. Zrnic, 1998: Discrimination between rain and snow with a polarimetric radar. *J. Appl. Meteor.*, **37**, 1228–1240.

Ryzhkov, A., D. S. Zrnic, and B. A. Gordon, 1998: Polarimetric method for ice water content determination. *J. Appl. Meteor.*, **37**, 125–134.

Straka, J. M., D. S. Zrnić, and A. V. Ryzhkov, 2000: Bulk hydrometeor classification and quantification using polarimetric radar data: Synthesis of relations. *J. Appl. Meteor.*, **39**, 1341–1372.

Vivekanandan, J., V. N. Bringi, M. Hagen, and P. Meischner, 1994: Polarimetric radar studies of atmospheric ice particles. *IEEE Trans. Geosci. Remote Sens.*, 32, 1–10.

Wallace, J. M. and P. V. Hobbs, 1977: *Atmospheric Science*: *An Introductory Survey.* Academic Press, 467 pp.

Wurman, J., J. Straka, E. Rasmussen, M. Randall, and A. Zahrai, 1997: Design and deployment of a portable, pencil-beam, pulsed, 3-cm Doppler radar. *J. Atmos. Oceanic Technol.*, **14**, 1502–1512.